Multistage radial flow pump - turbine for compressed air energy storage: experimental analysis and modeling

Egoi Ortego Sampedro, Antoine Dazin, Frédéric Colas, Olivier Roussette, Olivier Coutier-Delgosha, Guy Caignaert

▶ **To cite this version:**

Egoi Ortego Sampedro, Antoine Dazin, Frédéric Colas, Olivier Roussette, Olivier Coutier-Delgosha, et al.. Multistage radial flow pump - turbine for compressed air energy storage: experimental analysis and modeling. Applied Energy, 2021, 289, pp.116705. 10.1016/j.apenergy.2021.116705 . hal-03171002

HAL Id: hal-03171002
https://hal.science/hal-03171002v1

Submitted on 10 Mar 2023

HAL is a multi-disciplinary open access archive for the deposit and dissemination of scientific research documents, whether they are published or not. The documents may come from teaching and research institutions in France or abroad, or from public or private research centers.

L'archive ouverte pluridisciplinaire **HAL**, est destinée au dépôt et à la diffusion de documents scientifiques de niveau recherche, publiés ou non, émanant des établissements d'enseignement et de recherche français ou étrangers, des laboratoires publics ou privés.

Distributed under a Creative Commons Attribution - NonCommercial 4.0 International License

Version of Record: https://www.sciencedirect.com/science/article/pii/S0306261921002282
Manuscript_1a822ca6e49f0a9862c0e3a201aad9f9

Multistage radial flow pump - turbine for compressed air energy storage: experimental analysis and modeling

Egoï Ortego[1,2], Antoine Dazin[1], Frédéric Colas[3], Olivier Roussette[1], Olivier Coutier Delgosha[1,4], Guy Caignaert[1]

1 Univ. Lille, CNRS, ONERA, Arts et Metiers ParisTech, Centrale Lille, UMR 9014-LMFL-
Laboratoire de Mécanique des Fluides de Lille - Kampé de Fériet, F-59000, Lille, France.
2 MINES ParisTech-PSL Research University-CES, Palaiseau, France
3 Univ. Lille, Arts et Metiers Paris Tech, Centrale Lille, HEI, EA 2697 - L2EP - Laboratoire d'Electrotechnique et d'Electronique de Puissance, F-59000 Lille, France
4 Kevin T. Crofton Department of Aerospace and Ocean Engineering, Virginia Tech, Blacksburg, VA 24060, USA

Abstract

The increasing development of storage systems connected to electrical networks is stimulated by network management issues related to recent energetic landscape evolutions such as the increasing integration of renewable production sources. Hydro-pneumatic systems seem to offer a clean and cheap energy storage solution among the set of existing storage techniques. The present study analyses an air-water direct contact accumulation system, in closed cycle, using a rotodynamic reversible pump/turbine. The use of a unique energy conversion machine and easy-to-recycle materials could lead to cost-effective, environmentally friendly storage technique with long service life. The paper is focused on the experimental implementation and analysis of the system in a Lab environment, and the modeling of its multi-physic dynamic behavior. To deal with the variable operating conditions of the system, two different real time control strategies of the hydraulic machine were successfully tested. Finally, the global system efficiency is discussed. The efficiency control strategy was achieved with a 31% round trip efficiency and the power control strategy lead to 5% and 23% precision on exchanged power in charge and discharge modes respectively. The multi-physic dynamic model led to a 4% error of turbine mode acceleration prediction showing the interest of such a modeling method for such transient systems.

Nomenclature

Symbols

C_v	Constant volume specific heat (J/(kg.K))
D	Diameter (m)
f	Friction factor (kg.m²/s)
F	Shape factor
g	Gravitational acceleration (m²/s)
h	Heat transfer coefficient (W/(m²/K)))
H	Height (m)
I	Rotational inertia (kg.m²)
k	Torsional stiffness (N.m/rad)
K	Gain
L	Length (m)
m	Mass (kg)
M	Torque (N.m)
Nu	Nusselt number
P	Pressure (Pa)
Pu	Power (W)
$\dot{Q}$	Heat transfer rate (W)
q_V	Volume flow rate (m³/s)
r	Impeller radius (m)
$R2$	Maximum impeller radius (m)
$R_a{}^*$	Modified Rayleigh number
R_s	Specific gas constant (J/(kg.K)))
s	Laplace operator
S	Area (m²)
T	Temperature (K)
T_i	Integrator gain
t	Time (s)
V	Volume (m³)

Greek symbols and operators

Δ	Difference
β	Angle between relative flow velocity and tangential direction (rad)
β'	Coefficient of thermal expansion
δ	Flow coefficient
η	Efficiency
λ	Thermal conductivity (W/(m.K))
μ	Dynamic viscosity (Pa.s)
ρ	Density (kg/m³)
τ	Power coefficient
τ'	Thermal time constant (s)
ψ	Pressure coefficient
ω	Angular speed (rad/s)

Subscripts

$algo$	algorithm
amb	ambient
f	Final
h	High
i	Initial
L	Liquid
l	Low
P/T	Pump/turbine
ref	reference
st	storage
st_{turb}	Start turbine
sup	supervision
w	water

1. Introduction & positioning

Energy storage is one of the most promising solutions considered by power system operators to smooth the effects of current and future increasing stresses on electrical grids [1]. Although energy storage has various applications, it is especially impacting the on-going penetration of renewable energy sources in the existing electrical networks.

Several types of energy storage techniques are currently available. It includes Pumped Hydroelectric Storage (PHS), Compressed Air Energy Storage (CAES), electrochemical batteries,

© 2021 published by Elsevier. This manuscript is made available under the CC BY NC user license
https://creativecommons.org/licenses/by-nc/4.0/

and flywheels [2]. Nowadays, the most widely developed technique is PHS. This technique is extremely mature in terms of life time and cost management and represents 98% of the grid connected storage systems installed power [1] [3]. However, its development is limited in Europe by the lack of new sites, because of the needed water level difference and volume. The large-scale CAES represents a serious alternative to PHS [1] [4], however the currently installed CAES stations present the disadvantage of gas burning requirement during the expansion period [5]; besides the existing CAES stations use gas compressors and turbines with a limited number of stages and intercoolers avoiding any possibility of isothermal compression/expansion that lead to severe losses if the storage is not adiabatic. It is possible to recover a part of the compression generated heat to store it and use it for expansion; but it is quite challenging to extract and conserve the heat at high temperatures [6]. Adiabatic-CAES could be a solution to the heat management problem. Such a system was studied by RWE in Germany with the so called ADELE project [7]. The main difficulties for such adiabatic systems come from the high operation temperatures and pressures leading to challenging designs for the rotating parts and the heat storage systems operated at high pressure. The technology readiness level and affordability of the very specific components required needs still to be proven.

Hydro-pneumatic energy storage (HYPES) is a type of volumetric compressed air storage technique [8]. It intends to combine the good efficiency and technological maturity of hydraulic energy conversion with the spatial flexibility and large energy densities of compressed air energy storage in vessels. The HYPES basic idea is to compress air in a closed volume by means of a liquid piston during storage phase thanks to a pump and use this potential energy when needed to drive a turbine. Furthermore, the liquid piston concept presents a strong potential for the heat management all along compression or expansion making possible isothermal cycles. Such cycles don't need any heat storage and present higher energy densities than adiabatic cycles [8].

The idea of using liquids to compress air is quite old, as it has been firstly described by Mékarski at the end of 19th century [9]. It is also interesting reading the humid compressor patent of Dubois-François, in the same period, where the use of liquid water is proposed to improve the compression efficiency [10]. The concepts of liquid piston and spray cooling were new at that time. This air compression technique enables to perform a quasi-isothermal storage cycle, which has various advantages such as avoiding high temperature thermal storage, or energy sources (gas burning) and also higher energy densities [8].

For these reasons, closed or open volume hydro-pneumatic compression/expansion systems have been more recently studied by different teams. A team of the EPFL worked on a hybrid system based on oil hydraulic machines at pressures up to 200bar in a closed cycle [8]. The use of oil in such systems requires a separation membrane. The achievement of isothermal cycles using heat exchanger would be expensive at such pressures and prays injecting in a membrane are not technically obvious regarding cooling stream circulation. Achievement of such oil based liquid piston systems without membrane would require compatibility studies between oil and air at high pressures and temperatures for safety reasons. In general, water based systems are preferred by most teams working on isothermal compressed air storage systems This is the case of Sustain-X start up which developed water foam cooling based compressed air systems [11] and also the case of LightSail Energy start up which developed water spray assisted storage system [12]. These two companies objective was to attain isothermal cycles with large mechanical compression reciprocating devices. Unfortunately they both stopped their activity probably because of the excessive cost associated with the complex compression devices. Regarding water based hydro-pneumatic systems; a nice example is the case of the GLIDES project team in which a Pelton turbine was used for energy release and a centrifugal pump for storage [13]. This system was operating between 70bar and 100bar and needed a separated motor and generator.

In this context, a new concept for HYPES systems is presented in this paper. It is deliberately based on simple components like a centrifugal pump used as a turbine and water as fluid compression system. Both motor and generator functions are performed by a single asynchronous machine. At the best knowledge of the authors this is the first time this kind of hydraulic machine is used for HYPES. An illustration of the proposed system is presented in Figure 1.

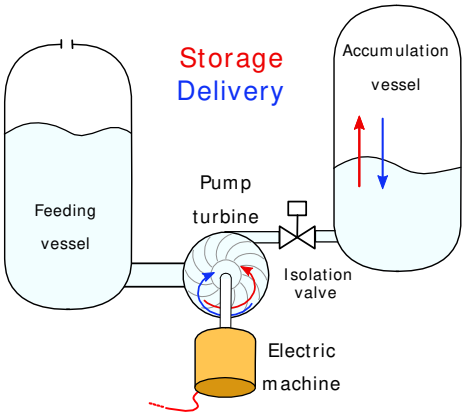

Figure 1: HYPES system using a reversible pump-turbine

This approach is a promising cost-effective solution, compared to other systems, as the initial investment is limited while it may enable an efficient management of the energy storage and recovery steps.

Indeed, the use of a centrifugal pump enables to minimize the development costs, since pumps are very usual components and a single electric machine is needed. Moreover, the use of water instead of oil lowers the environmental impact, and the materials are also easier to recycle. Working at lower pressure (maximum of 40bar in the present case) could also decrease the design cost of the system, since a large variety of components can be found for operation with water up to 63bar.

Nevertheless, using a radial flow open machine in conditions of variable pressure is a major challenge. Besides, the pneumatics, hydraulics and mechanics of the system are strongly coupled, which makes the estimation process of the characteristic times very challenging. However, this information is crucial for the assessment of the system performance and the comparison of various storage devices. Furthermore the strong coupling between the components make the control of the system quit challenging when trying to maintain a given power demand for example; this is related to the pressure dependent non-linear relation between machine's flow rate and angular velocity.

In order to handle these challenges, the performance of the new system is investigated in this study by a combination of original simulations and validations on a test rig. The simulations are based on a dynamic multi-physics model that simulates the transient behavior of a lab scale proof of concept prototype, and eventually provides a fine prediction of the response time of the system. It has to be pointed out that to the authors' knowledge, whereas such systems always operate in transient conditions all the existing models are based on a quasi-steady assumption. The development of a dynamic model is thus necessary to predict accurately the behavior of the system.

The lab-scale prototype was specifically developed to provide the appropriate data for the validation of the model. Besides, a novel real time supervision algorithm was developed for the storage-recovery cycles using the multi-physic dynamic model in order to numerically test different control strategies. The algorithm was then implemented in real time operating conditions on the test bench. It was developed to control the HYPES device either in best operating point mode or in a power request mode with variable pressure operation. This framework paves the way to design future systems based on the proposed principles in this paper.

Besides, even if a lot of air based energy storage systems have been studied in literature, very few experimental research papers deal with compressed air energy storage. For example in a very recent research review [14] only 2 referred papers deal with CAES end-to-end (i.e. round trip cycle) experimental results; one of them refers to Huntorf plant and the other is the heat storage assisted CEAS cited above in the introduction [6]. So the present paper aims to contribute in HYPES systems knowledge by the technical feasibility demonstration of a novel HYPES system, by a novel real time control technique and by a multi-physics dynamic model.
The paper is organized as follows: the modeling of the system, based on dynamic mass, momentum and energy balances, is first detailed, then the test rig is presented, including the experimental calibration of the accumulation vessel heat transfer coefficient. Finally, the experimental and simulated data of two storage-recovery cycles with different control strategies are presented and discussed.

2. HYPES modeling

The proposed model aims to predict the dynamic behavior of the storage device. The components of the HYPES system studied here are presented in Figure 1: an accumulator, a pump-turbine, an electric motor/generator controlled by a frequency inverter, a valve and a feeding vessel.

The model is composed of sub-models for each component and a supervision algorithm. Three main physical domains are modeled: mechanical, hydraulic and thermodynamic domains. The coupling between these domains makes the model multi-physic.

The system modeling is performed with Matlab/Simulink that accepts only a low number of algebraic loops. That's why the equations are written in order to avoid them by using a causal modeling approach. This allows a fast and simple time integration to solve the system. Each sub-model describes the behavior of the considered part as an assembly of basic inertial, capacitive or resistive elements.

Figure 2 displays the structure of the global model. The input/output variables of each sub-model are represented by the solid arrows. The dashed blue arrows represent input variables for the control; the red dashed arrows represent controlled variables. The supervision program has been developed with Sateflow in Matlab/Simulink and is detailed in section 2.5.

The central sub-model is the hydraulic sub-model; many of others interact through this one. Pressures are applied on it and it computes the flow rate which is an input for other sub-models. The status of the valve is ordered by the supervision program based on the storage cycle requirements and is depending on the actual flow rate value (this aspect is discussed in section 2.5).

The rotating bodies sub-model was designed in order to model the dynamics of the shaft in conjunction of the frequency inverter controller dynamics. One of the design criteria was to allow the ''freewheel'' mode operation in which the supervision program reference velocity (ω_{ref}) is omitted and the shaft velocity depends only on hydro-mechanic dynamics allowing to estimate the natural response time of the turbine mode. The mechanical sub-model interacts with the hydraulic sub-model through the pump-turbine model as show in Figure 2.

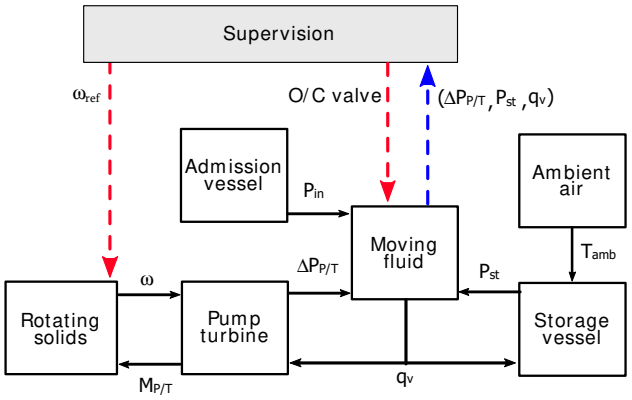

Figure 2: global bloc diagram; sub-models input/output variables and control/controlled variables

Each sub-model is described in more in detail in the following paragraphs. The equations for each component dynamic behavior are provided and the relations between the components are presented in the form of transfer functions to lighten the way of presenting the global mathematical formulation of each sub-domain.

2.1. Mechanical sub-domain

The aim of this sub-model is to predict the angular speed of the rotating solids i.e. the pump/turbine and the motor. The model for the mechanical system is based on two inertial elements (the motor and the pump/turbine) and a capacitive element representing the torque sensor, considered as an elastic component connecting the two rigid elements (see Figure 3).

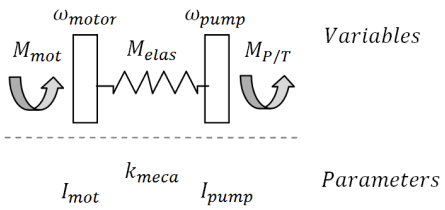

Figure 3: model of the mechanical system

The time derivative of the angular speed (ω) of rotating masses is related to the torques applied on them, as expressed by equation (1).

$$\frac{d\omega}{dt} = \frac{\Sigma M}{I_{Oz}} \quad (1)$$

Where I_{Oz} is the angular inertia of the considered element and ΣM the sum of the torques applied on it:

- The electromagnetic torque (M_{motor}) and the elastic torque (M_{elas}) for the motor shaft
- The hydraulic torque received or applied by the pump/turbine ($M_{P/T}$) and the elastic one (M_{elas}) on the pump shaft.

The behavior of the elastic element used to estimate the elastic torque is described by equation (2).

$$\frac{dM}{dt} = \frac{\omega_{motor} - \omega_{pump}}{k} \quad (2)$$

Where k is the torsional stiffness of the parts between the motor and the pump.

The overall transfer function of the mechanical sub-model is shown in Figure 4.

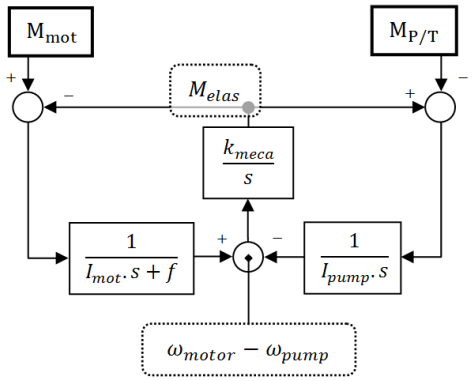

Figure 4: transfer function of the mechanical sub-model

The two ''input'' torques (thicker lines boxes in Figure 4) are deduced from:

- The pump/turbine model discussed hereafter
- A PI (proportional integral) controller (see appendix 7.1) that compute a driving electromagnetic torque value as a function of a reference speed (ω_{ref} in Figure 2) and the configured dynamic response parameters.

The time integration of equations (1) and (2) from their initial states provides the values of the angular speed and the elastic torque.

2.2. Hydraulic sub-domain

The hydraulic sub model describes the dynamics of the fluid (water) contained in the pipes and the hydraulic machine. A simplified form of the momentum equation is used to predict the flow rate (equation (3)) as a function of the pressures applied on the equivalent water column. The initial derivation of the equation can be found in the work of Nicolet [15] on the unsteady behavior of hydroelectric systems.

The hydraulic inertia of this water column is named I_L. We consider here water as incompressible and the pipes are assumed to be rigid.

$$\frac{dq_V}{dt} = \frac{1}{\boldsymbol{I_L}}.\Delta P_{balance} \quad (3)$$

The balance of the pressures applied to the water column ($\Delta P_{balance}$) is detailed by equation (4).

$$\Delta P_{balance} = P_{in} + \Delta P_{P/T} - P_{accu} - \Delta P_{val} - \Delta P_{fric} \quad (4)$$

The accumulator pressure (P_{accu}) is an input variable computed in the reservoir model. The pump/turbine pressure difference ($\Delta P_{P/T}$) is computed by its corresponding sub-model (see section 2.3). Frictional pressure losses (ΔP_{fric}), on pipes, junctions and filter, depend on the flow rate, and they are derived from literature [16] and experimental observations performed by the authors [17]. In the later reference, detailed information on the sub model used to compute the pressure at the suction pipe inlet (P_{in}) can also be found.

The isolation valve is modeled as a pressure source (ΔP_{val}) responsible for the flow rate stopping when needed. The value of the pressure applied by the valve is computed by a PI controller based on the dynamics of the hydraulic circuit. The main asset of this method is to avoid residual flow rate involved in classic valve models, for all stand-by and operating pressure conditions. See appendix 7.2.

The overall fluid inertia (I_L) is the sum of various elementary inertias. The pipes are modeled as cylinders of cross section area S and length L; their hydraulic inertia is equal to $\rho_w.L/S$.

It can be noticed that the hydraulic inertia related to the flow rate is inversely proportional to the cross section area. That is why the inertia of the water contained in both vessels is very small.

For the pump/turbine, the inertia for a wheel is evaluated with equation (5) [18].

$$I_{wheel} = \frac{\rho_w}{4\pi}\int_{R1}^{R2} \frac{1}{r\, b(r)\, sin^2\beta(r)}\, dr \quad (5)$$

12 wheels are accounted for the overall inertia. The impeller internal and external radii are denoted R1 and R2. The function $b(r)$ represents the blade width evolution; it was considered

constant here. The blade angle $\beta(r)$ was supposed to be a linear function between the impeller inlet and outlet angles.

The global transfer function of the hydraulic model is described in Figure 5.

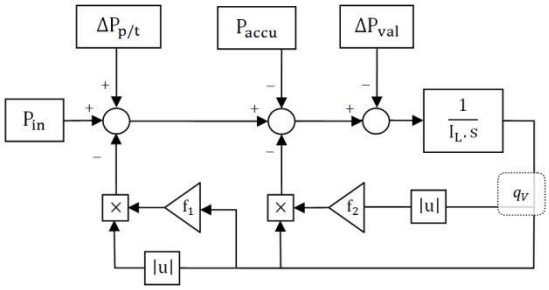

Figure 5: hydraulic model transfer function

2.3. Pump/turbine model

The pump/turbine behavior is modeled by its steady operating charts shown in Figure 6 and Figure 7. The dimensionless pressure (ψ), power (τ) and efficiency are drawn as functions of the dimensionless flow rate (δ) computed with the system of equations (6). Efficiency was plotted with dotted lines and values are in the right axis.

$$\begin{cases} \delta = \dfrac{q_V}{R2^3.\omega} \\ \psi = \dfrac{\Delta P_{p/t}}{\rho_w.R2^2.\omega^2} \\ \tau = \dfrac{Pu_{mecha}}{\rho_w.R2^5.\omega^3} \end{cases} \quad (6)$$

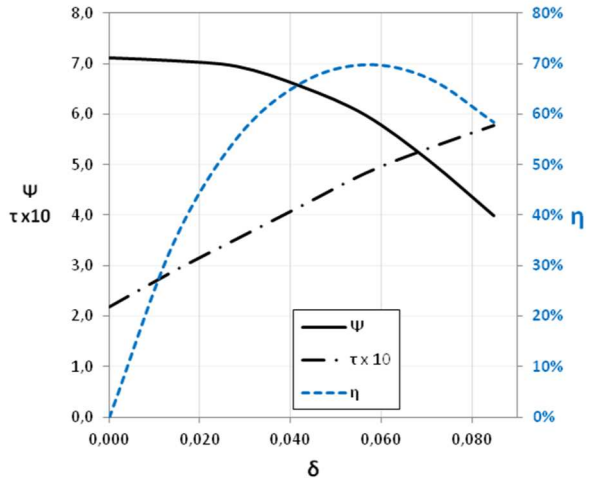

Figure 6: pump characteristics

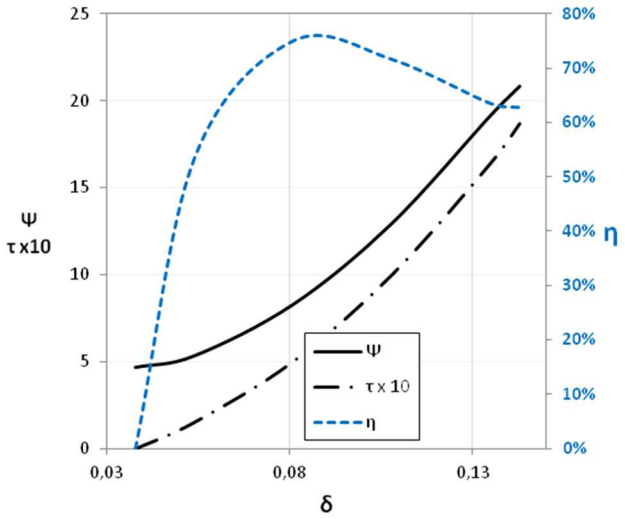

Figure 7: turbine characteristics

The relations between the dimensionless parameters values are modeled using the two polynomial expressions (7) and (8).

$$\psi = A1 + A2\,\delta + A3\,\delta^2 \quad (7)$$

$$\tau = B1 + B2\delta + B3\delta^2 \quad (8)$$

For low rotation speed operating conditions viscous nonlinear effects become relatively more important and a deviation from the presented curves is observed due to Reynolds effects. For these conditions, the pressure and the torque coefficients could be better modeled by a series of curves (one per angular velocity sector) or by 2D tables of the form $\psi = f(\delta, \omega)$. Deviations could also be observed at higher pressure levels, because of lower volumetric efficiencies.

2.4. Accumulator model

The objective of this sub model is to predict the global thermodynamic behavior of the accumulator; the main parameters responsible for the energetic state of charge are the

mean temperature and the pressure of the compressed air. The direct air-water contact leads to mass transfer phenomena. Interface transfer mechanisms were treated by local models detailed in [17]; the main conclusion is that the air mass variation, for a 20 bar initial pressure, is less than 4% after 80 days of standby with stagnant water in contact with air; the air mass was thus considered constant. At the same time, the distance between the interface and the reservoir connection pipe was found sufficient to avoid any turbine performance degradation by air intrusion.

Air was considered as an ideal gas because of the relatively low operating air densities (pressures are below 20bar and temperature between -20°C and 70 °C).

Energy conservation is applied to the air mass contained in the accumulation volume as expressed in equation (9).

$$m.C_V.\frac{dT}{dt} = \dot{Q} - P.\frac{dV}{dt} \quad (9)$$

Where P is the air average pressure. The pressure P_{acc} is equal to P plus the water column height. The air volume is denoted V. The work introduced in equation 9, last right-hand term, is a function of the air mean pressure and the volume variation rate of the air; this last term is equal to the water volume flow rate (with an opposite sign), since water is considered as incompressible. The heat transfer rate ($\dot{Q}$) is related to the thermal transfer between the air and its surrounding.

Equation 9 will be used to predict the air mean temperature (T). The relation between the pressure, the volume and the temperature is obtained by the perfect gas equation (10).

$$P.V = m.R_S.T \quad (10)$$

Where m is the mass of air and R_s the air specific gas constant.

Since the components in contact with air (the metallic walls of the reservoir and the water) are characterized by large heat capacities, the temperature of the interface between air and its surrounding is considered as constant and homogeneous. This assumption was compared to a situation where all the heat generated by the compression would contribute to the temperature increase of the metallic wall. The two situations gave the same heat transfer rate within a few percents. On top of that, the maximum measured variation of the wall external temperature was about 1.5K, i.e. less than 2% of the maximum air temperature.

The heat flow is thus calculated by equation (11).

$$\dot{Q} = h.S.(T_i - T) \quad (11)$$

The internal convective heat transfer coefficient (h) takes into account the flow through the water such as the one through the metallic wall; it was experimentally determined by a thermal time constant measurement method [19]. The detail of this method and the results for our specific vessel are presented in section 3.3.

2.5.Supervision algorithm

A storage cycle is composed of three periods: accumulation, standby and delivery.

The two active periods are characterized by variable operating conditions in the present configuration. It requires the control of the angular velocity of the pump/turbine in order to maintain the required flow rate and/or efficiency conditions. Two main configurations were tested for the angular speed control: best efficiency point (BEP) and power control (PCT) configuration. The first computes a BEP angular speed by using the instantaneous value of the pressure difference at the pump/turbine inlet and outlet and the BEP point dimensionless pressure value (ψ_{BEP}) (see BEP in Table 1). The ψ_{BEP}value is obtained from the pump and turbine performance tests.

Table 1: angular speed reference configurations for the supervision program

BEP	$\omega_{algo} = \sqrt{\frac{\Delta P_{P/T}}{\psi_{BEP}.R2^2.\rho_w}}$	(12)
PCT	$\omega_{algo} = f(Pu_{ref}, \Delta P_{P/T})$	(13)

The second reference speed is based on a lookup table in which the inputs are the value of the required mechanical power and the pump/turbine pressure difference value (see PCT in Table 1). The look-up tables are presented in appendix 7.3.

The supervision program state machine is presented in Figure 8.

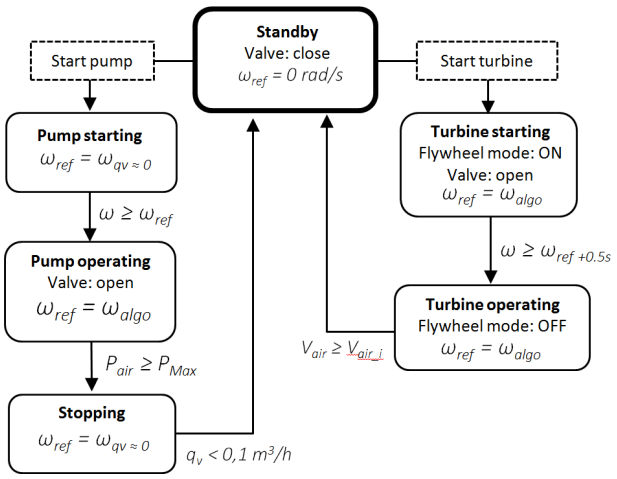

Figure 8: supervision state diagram / observed and controlled variables

The observed variables were the actual motor angular speed, the storage vessel pressure and the mass flow rate. The controlled variables were the reference angular speed and the valve state.

The main particularity of the presented supervision program is related to the velocity management during start-up periods. Before the main ''Pump operating'' step, the standby pressure in the accumulator can be superior to the one of the pump inlet. Therefore, to avoid a rapid discharge, the pump was activated before opening the valve in order to reach a sufficient pressure; this is the role of the ''Pump starting'' step. For that situation, the

reference speed is named $\omega_{q_V\sim0}$; its value is based on the dimensionless pressure observed in zero flow condition ($\psi_{\delta\sim0}$).

$$\omega_{q_V\sim0} = \sqrt{\frac{(P_{st} - P_{atm})}{\psi_{\delta\sim0}.\,\mathrm{R}2^2.\,\rho_w}}$$

The increase of the angular speed of rotation is limited to 270tr/min per second.

The ''Stopping'' step activates when the maximal pressure is reached in the storage vessel. This step triggers a decrease of the pump velocity to set the flow rate to values close to 0 and when the flow rate reaches its minimum threshold value (0,1m³/h), the valve is closed.

In the case of the turbine mode start-up, in order to avoid energy consumption during discharging, an auto-start-up situation was favored: first, the turbine is only driven by the torque produced by the water flow subsequent to the valve opening. The electric generator torque is zero: freewheel is active. When the angular speed is sufficient (close to the one of the maximum efficiency point), the ''freewheel'' mode is turned to inactive; then the power supply begins. The turbine is stopped when the air volume gets back to its initial value.

3. Equipments and methods

In this section are presented the components of the test rig, the physical parameters used for the modeling of each component and an example of a component characterization: the identification of the storage vessel thermal behavior.

3.1. Equipments

A schematic view of the developed prototype is shown in Figure 9. A picture of the test rig during the assembly phase is shown in Figure 10.

The test rig is composed of a Siemens bipolar 70kW squirrel cage asynchronous machine and an inverter including an Active Front End module (AFE), a KSB Multitec A50/12A reversible 12 stages pump, a storage steel vessel (40bar i.e. 280Wh/m³ max capacity), a feeding vessel and a pneumatic control ball valve. The inverter freewheel mode is controlled by a digital input and the reference velocity by an analog input.

The piping includes a DN100 pipe connecting the feeding vessel to the pump suction side, a DN40 pipe which connects the pump outlet to the storage vessel and an auxiliary return pipe. This last pipe is used only for steady pump performance characterization; the vane on this pipe is a variable section valve that allowed setting several steady operating conditions. The storage vessel can be fed with compressed air up to 8bar in order to achieve pre-charged compression/expansion cycles. The storage vessel had a 1m3 volume leading to maximum design storage energy of 280Wh.

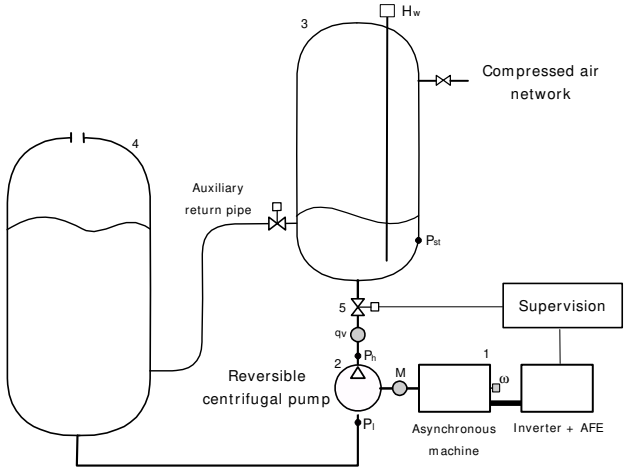

Figure 9: test rig main components and instrumentations; 1-electric motor/generator, 2-reversible pump turbine, 3-storage vessel, 4- feeding vessel, 5-control vane

Figure 10: view of the test rig

Table 2: list of measuring instruments

Variable	Type of sensor/transducer	Conditioning	Uncertainty
Flow rate	Bidirectional electromagnetic: Proline Promag 50W. Hendress & Hausser.	4-20mA	0.2%
Absolute static pressure	Piezoresistive : PAA 33X. Keller.	RS-485	0.025%FS
Torque	Torque transducer : T30FN/500 N.m + MD18N amplifier. HBM.	±10V	Error band <0.08%
Angular speed	Motor integrated encoder: 1024 pulses per rotation.	±10V	
Internal temperature	PT100 sensor: HC2-IE102 + HF532 transducer. Rotronic.	4-20mA	±0.1K at 23°C
Water level	Guided radar level meter: Optiflex1300. Krohne.	4-20mA	±3mm

Surface temperature	Type K Thermocouple.	0-10V	±2K (due to EMI noise)

The sensors used on the test rig are presented in Table 2. Their positions and associated variables are presented in Figure 9: the pressure transducers (P_l and P_h), the flow meter (q_v), the torque transducer (T), the water level transducer (H_w) and the encoder on the motor shaft (ω). Data acquisition and generation of the control signals was performed with a National Instruments PXIe system with various PXI slots. The inverter was configured on vector control mode including real angular velocity signal. The supervision program was implemented in Labview. The control algorithm was executed at a frequency of 60Hz and a complete cycle duration was of the order of 90s.

3.2. Components' physical parameters

The test rig was used for the empirical tuning of the simulation model parameters; the main experimental studies were focused on:

- The steady state performance in the pumping mode
- The quasi steady performance in the turbine mode
- Internal natural heat convection coefficient of the storage vessel
- Motor/generator friction factor
- Pump/turbine mechanical inertia
- Low pressure vessel dynamic behavior

The tuning procedures for these parameters are detailed in [17]. The resulting characteristics of the different components are presented hereafter.

Regarding the mechanical components, the empirical relation obtained for the motor natural friction factor has this form:

$$f = 0{,}336.\,\omega^{-0{,}64} \qquad (14)$$

The values obtained for the inertias and the torsional stiffness are the following:

I_{mot}	I_{pump}	k
0.717 kg.m²	0.15 kg.m²	95 kN.m/rad

The values I_{mot} and k were provided by the manufacturers. The constants of equation (14) and the value of I_{pump} were obtained by free deceleration tests.

Regarding the hydraulic components, the retained hydraulic inertias are given in Table 3:

Table 3: hydraulic inertias in **kg/m⁴**

Low pressure pipe	High pressure pipe	Pump wheels	Pump diffusers	Storage vessel	I_L(total)
$1.81.10^5$	$7.36.10^5$	$8.33.10^5$	$2.02.10^5$	$5.62.10^3$	$1.96.10^6$
9%	38%	43%	10%	0.3%	

The pump was characterized for different fixed angular speeds at different pressure levels in purely steady situation in a closed loop test configuration as mentioned before.

The turbine mode was characterized during quasi-steady operating conditions driven by the slow expansion of pre-compressed air flowing water out of the high-pressure vessel. Quasi-steady condition means that the effects of the hydraulic and mechanical accelerations are small. These effects can increase during fast start-ups of pumps for example and may affect noticeably the performance curves [18]. In the present case, according to the observed flow rate and angular velocity accelerations, these transient effects result in less than 3% of variation of the steady torque and pressure difference.

The values obtained experimentally for the constants in equations (7) and (8) are given in Table 4. These values are valid within a range of 5% for rotational speeds higher than 750rpm for the pump and the turbine.

Table 4: pump and turbine constants

	Pump			Turbine		
	1	2	3	1	2	3
A	6.89	25.4	-810	4.94	-46.29	1196
B	0.21	6.6	-23.1	-0.188	-0.226	99.16

The presented dimensionless curves (§2.3) and associated constants are valid for pressure differences ranging from 5 to 25bar.

The presented numerical values are specific for the specific test bench used in the present study. Nevertheless, the majority of inertial terms are scalable and the main frictional parameters are easy to estimate. A change in power rate would need to introduce the constants of the new hydraulic machine and it is generally feasible with the manufacturer data. Regarding the storage vessel, the change in energy capacity would need to adapt the volume and heat transfer area. Regarding the heat transfer coefficient, a method to measure it and an example is presented below.

3.3. Accumulator heat transfer coefficient

Hereafter is presented an example of physical characterization of a component.

The accumulator is one of the key components of the HYPES system. In a closed system, the dynamics of compression, expansion and stand by periods depend on the state of the air in the accumulator.

After a compression period, if the air temperature is different from the one of its surroundings, during a workless period ($\mathrm{d}V = 0$), the thermal equilibrium is reached at a rate depending on the thermal capacitance of the air mass ($m_{air}.C_v$), assuming that the temperature variation of the metal and water is negligible, and on the global heat transfer capability (h.S), analogue to the inverse of the resistive element in a RC electric circuit.

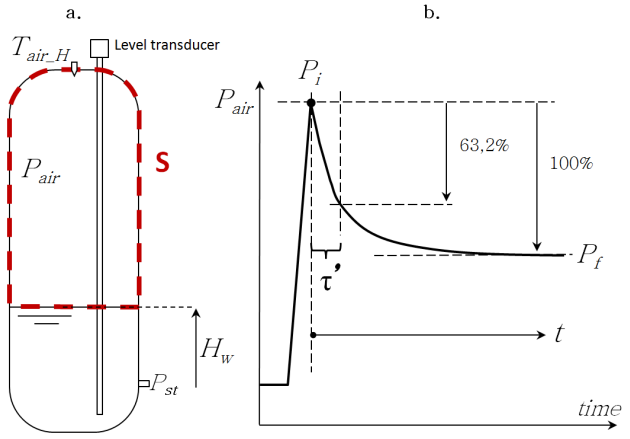

Figure 11: a-storage vessel; b-pressure change during a compression - cool down period

Assuming a perfect gas behavior, a constant exchange surface mean temperature (T_S) the relaxation rate of the mean air pressure can be expressed with a decreasing exponential function given in equation (15).

$$P_{air} - P_f = (P_i - P_f).e^{-\frac{t}{\tau'}} \tag{15}$$

The final thermodynamic equilibrium state is defined by the final pressure (P_f related to the final temperature supposed equal to T_S and supposed here equal to the initial air temperature). The time constant (τ) is expressed as follows:

$$\tau' = \frac{m_{air}\, C_v}{h_g\, S} \tag{16}$$

The time constant can easily be measured by analyzing the mean pressure, or temperature, history after a compression or expansion period (Figure 11 b). This thermal time constant method to compute global heat transfer coefficients on pneumatic accumulators, used in hydraulic circuits, was developed by Purmovahed & al. [19].

The mean air pressure is calculated by measuring the accumulator pressure at its bottom part (see P_{st} Figure 11 a), from which a water column pressure is subtracted ($\rho_w g H_w$).

The air mass is supposed to be constant, and it is calculated before the heating/cooling periods, in a thermal equilibrium situation, assuming a perfect gas behavior and using the measurement of the initial volume, pressure and temperature. The initial temperature is measured by a sensor located at the top of the accumulator (see T_{air_H} Figure 11 a). The water vapor mass is neglected.

$$m_{air} = \frac{P_i V_i}{R_S T_i} \tag{17}$$

The expression of the global internal natural convective heat transfer coefficient is given by equation (18) as a function of the thermal time constant computed from the time history of the pressure (Figure 1-b).

$$h = \frac{m_{air}.C_v(T)}{\tau'.S} \tag{18}$$

The global heat transfer coefficient is then computed in its dimensionless form, the Nusselt number (Nu, see eq. (19)), in order to obtain a general empirical expression related to the parameters representative of the system state: a modified Rayleigh number (Ra* see eq. (20)) [19], ratio between buoyancy and viscous forces acting on air, and a geometric form factor (F see eq. (21)), useful to describe the possible end effects on the thermal transfer pattern.

$$Nu = \frac{h.L}{\lambda(T)} \tag{19}$$

$$Ra^* = \frac{{\rho_{ait}}^2.g.\beta'.(T_{air} - T_S).L^3.C_v(T)}{\mu(T).\lambda(T)} \tag{20}$$

$$F \equiv \frac{V}{S.D} \tag{21}$$

The air average transport properties are computed at the mean air temperature calculated from the mass, volume and pressure information at time $t = \tau$. The relations used to estimate these properties were those used at atmospheric pressure and only dependent on temperature since pressure variations remained relatively modest in the configured tests. Details of the pressure effects on the air properties can be found in the literature (see for example: [20], [21], [22]).

The empirical relation between Nu and the other parameters is obtained by a linear regression done on the logarithms of the variables using R programming language [23]. The subsequent expression for the Nusselt number is given by equation (22).

$$Nu = 3{,}25.Ra^{*0{,}272}.F^{0{,}765} \tag{22}$$

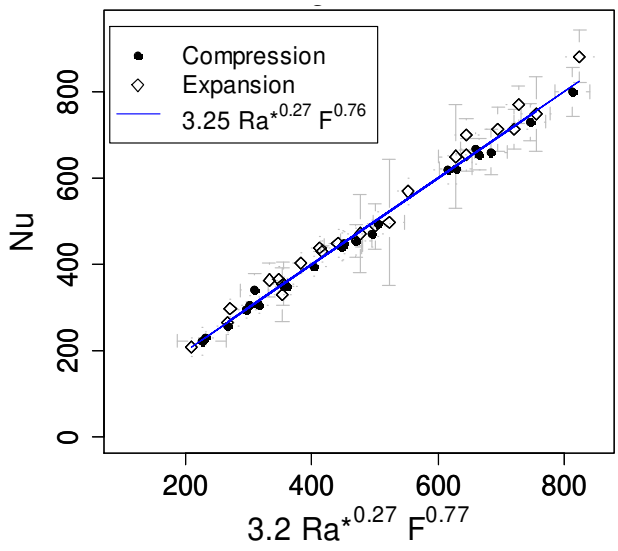

Figure 12: measured Nu compared to the regression line

Figure 12 shows the measured Nusselt number as a function of the Nusselt number computed by the expression (22) using

experimental Ra* and F values. It shows that the obtained empirical expression is consistent with the measured values within a maximum 10% discrepancy. The incertitude bars represent the result of an uncertainty propagation study made for the three parameters used in the expression and based on the measurement and data processing method; details of this analysis are given in [17].

It can be noticed that the cooling and heating Nusselt number values are very similar. This agrees with natural convection behavior on vertical surface as presented in [24] (section 9.4).

In the next section the experimental procedure and results are presented.

4. Storage performance tests

Various storage cycles were conducted in order to test different control strategies.

4.1.1. Analysis of BEP cycle

An example of results obtained in the case of a BEP cycle is first presented. The experiment was performed with the initial conditions and parameters indicated in Table 5. Note that the turbine start up is activated manually in the test bench, so the starting time is included as a parameter for the simulations.

Table 5: initial conditions for the BEP cycle

$V_{air\ i}\ (m^3)$	$P_{air\ i}\ (Pa)$	$T_{air\ i}\ (°C)$	$P_{Max}(Pa)$	$t_{st\ turb}(s)$
0.51	9.10^5	18	$12.5.10^5$	64.5

These initial conditions were used to run the model presented in section 2.

The evolutions of the key parameters during a cycle are analyzed hereafter.

The angular speed of the pump/turbine is an essential parameter of the system, since this is the only controlled continuous variable responsible for the operating conditions. It is also the parameter that defines the time response of the storage system in case of a sudden energy request.

Figure 13 displays the angular velocity observed and calculated by the model. The reference velocities of the Simulink model supervision program and the one of the experimental supervision system are also provided.

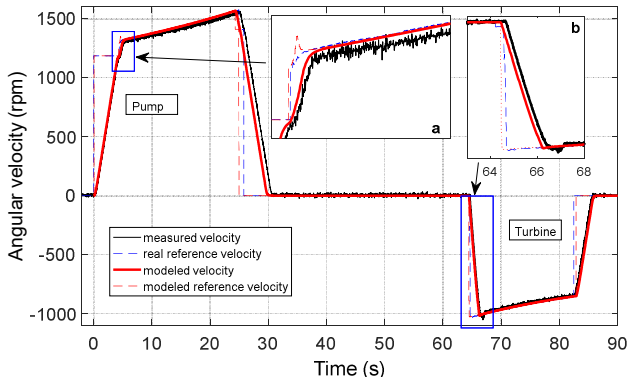

Figure 13: angular velocity

During open valve active periods, the difference between the observed and modeled reference velocity is lower than 3rpm (Figure 13). It implies a very good prediction of the pressure difference used as reference for efficiency control (eq. (12)) and thus a good hydraulic model quality. This can also be observed on Figure 14 where the measured and predicted flow rates are shown.

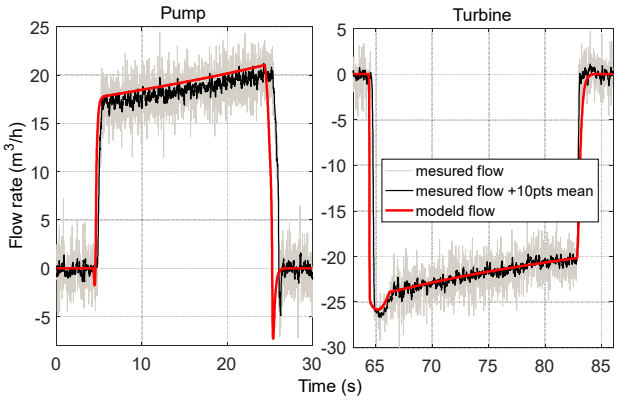

Figure 14: water flow rate

Figure 14 shows a predicted flow rate higher than the measured one; the data analysis showed that it was produced by an erroneous gain on the velocity reference sent to the inverter (see the difference between the reference speed of Labview and the real velocity in Figure 13 a.). Since the effective angular speed is lower than it should, the resulting pump pressure is lower, so it induces a lower flow rate. As a consequence, the maximal pressure is prematurely attained in the simulation (second 25 in Figure 14). At the end of the pumping period and at the beginning of the turbining period, the flow rates variation rates are very similar to the observed ones; this was made possible by the elaborated valve model. Besides the valve closing in conjunction to pump velocity reduction during the ''Stopping step'' (see Figure 8) worked well since flow annulations was achieved at very low torque and with very small back flow inducing no visible pressure drop in the vessel and thus very small energy losses.

During freewheel turbine start period, the acceleration was correctly predicted. This is a result of a good hydraulic turbine torque prediction; certainly due to a relatively good prediction of the flow rate in terms of order of magnitude and acceleration.

For this particular system, it seems that the hydraulic acceleration is largely higher than the mechanical one; thus the main parameter responsible of the time response of the device are the mechanical inertia and the torques applied on it. This shows the interest of multi-physic dynamic model since in such a coupled transient system this kind of information would be completely missing in a basic model.

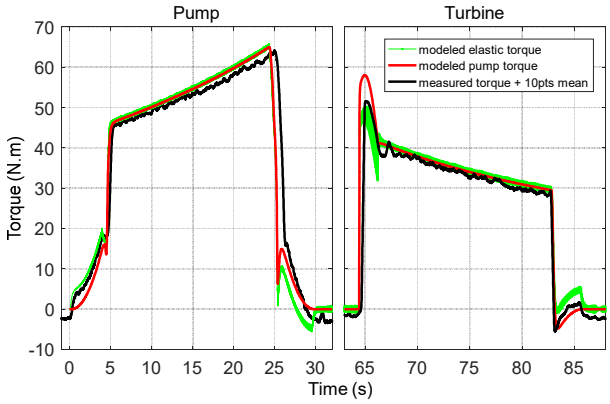

Figure 15: various torques

The measured torque is compared to the modeled pump torque and to the elastic torque (see Figure 15).

Two main parameters act on the torque value: the angular speed variations and the power transfer. The effect of the first can be observed is the first seconds of each startup where the elastic torque model changes at rates similar to the ones observed by the torque meter.

The accumulator pressure is shown in Figure 16. The difference between the modeled and observed values is about 8500Pa at the end of recovery period (t=83s) (less than 1 % of the measured value). That means that the computed air mean temperature is very close to the real one. Thus it can be concluded that the heat flows (dependent on the heat transfer empirical correlation) and the air volume variation rate are well predicted. The correct air pressure prediction contributes to the good prediction of the turbine stat up flow rate and the subsequent angular response time discussed before.

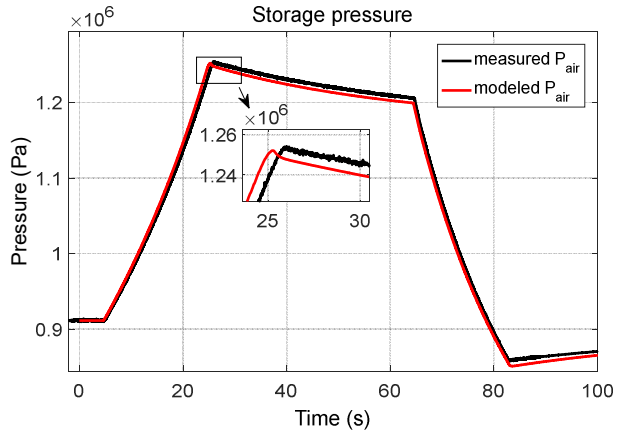

Figure 16: storage pressure

A slight pressure decrease is observed in simulation at the end of pumping period; that was related to the water backflow during the vane closing. This backflow was higher on simulation results than in the reality (see Figure 14, t≈25s) and produces an increase of the air volume.

A good evaluation of the pump/turbine's instantaneous efficiency can be obtained by expression 23.

$$\eta_{P/T} \approx \frac{\min[|M\ \omega|\ ;|\Delta P\ q|]}{\max[|M\ \omega|\ ;|\Delta P\ q|]} \qquad 23$$

The torque M is the one of the pump/turbine in the simulation and the measured torque for the empirical efficiency. That means that instantaneous efficiency comparisons can only be done during quasi-steady operating periods.

The time evolution of this efficiency is presented in Figure 17 and compared to the computed values. The pump was better modeled than turbine for which an efficiency discrepancy of 5 percent is observed; that seems to be related to a turbine torque over estimation.

Furthermore, despite the continuous pressure variation, the efficiency is maintained close to its optimum by the management of the angular velocity. This optimization does not prevent the system from the main energetic loss produced by the hydro-mechanic conversion.

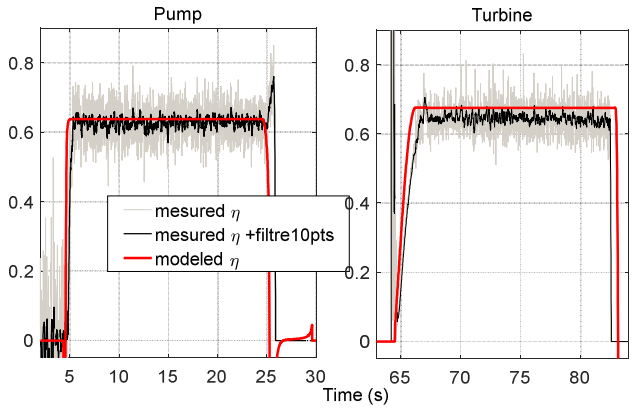

Figure 17: pump/turbine efficiency: BEP mode

Electrical power was given by the frequency inverter. Electrical conversion was not modeled here, thus it was roughly estimated by multiplying the speed control loop generated torque (that should be similar to the electromechanical one) and the angular velocity computed by the motor inertial model. The modeled and observed electrical powers are show in Figure 18; the ratio between both gives the efficiency of the asynchronous machine. That is why in pumping mode the measured values are higher than the modeled ones and in turbine mode the opposite is observed. Its value is around 87%.

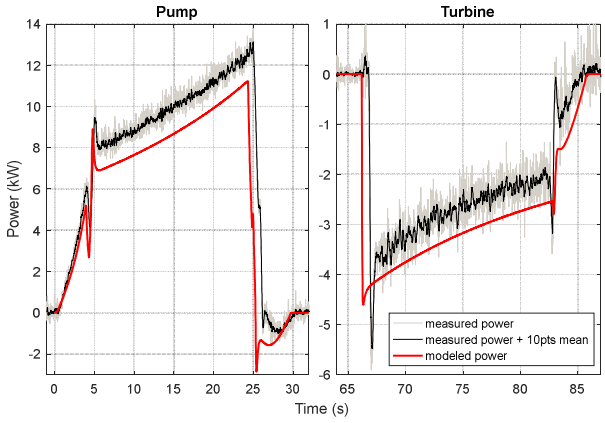

Figure 18: measured electrical power; modeled electromechanical power

A summary of the cycle's energy flows is presented in Figure 19. The fraction of the initial energy still available at different cycle

steps is in red. The efficiency of each step is in blue. Energy was obtained by time integration of power.

The main energy losses occur during pumping and turbining. This could be improved choosing machines with better efficiencies than the ones used in the present studies. This could be certainly possible at higher design powers.

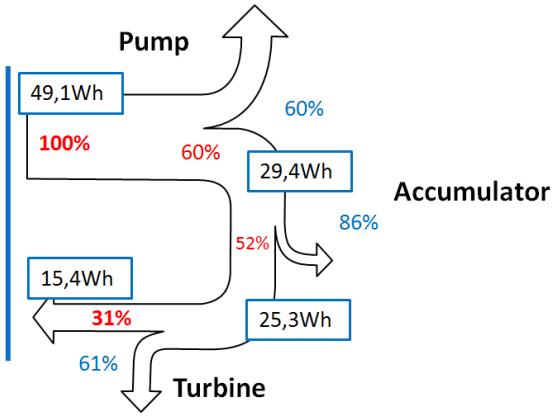

Figure 19: energy flow over a cycle (electric conversion not included)

The losses in the accumulator are small compared to the hydraulic conversion losses. However, these can be easily reduced by water injection in the vessel in order to get a process close to an isothermal cycle.

Table 6 gives a comparison between measured and modeled values of some important parameters of the system. It confirms the reliability of the prediction of the model, already observed on the instantaneous evolution of the parameters.

Table 6: a comparison between model and measurements

	Measured	Modeled	Discrepancy
Cycle shaft efficiency	31%	33%	+6%
Turbine unconstrained start up acceleration (rpm/s)	581	559	-4%
Turbine start pressure (bar)	12,06	12	-3% (referred to $P_{air_{init}}$)

For comparison purposes, some compressed air storage systems efficiency experimental values are reported here. The efficiency of the two well-known Huntorf and McIntosh CAES plants are respectively of 42% and 54% [4]. They were open systems operating around 50bar to 70bar and they presented the particularity of using gas combustion before expansion to reheat the air. . A Chinese team did a very interesting experimental work on this CAES with 108°C thermal storage; the observed round trip efficiency was 22.6% [6]. The main discrepancy to the expected value was due to the poor heat recovery during compression. For the GLIDES project the shaft efficiency was 30% [13]; this was a closed HYPES system operating between 70bar and 100bar. Lemofouet-Gatsi obtained an efficiency of about 43% [8] with a closed HYPES system operating between 100bar and 200bar and oil hydraulic machines. The only system using a reversible machine was the last one. Another recent research paper presents a 15% efficiency (including thermal power) for an open compressed air storage system operating at 300bar where a multistage compressor and an air motor were used [25].

The efficiency of 30% of the present system thus appears rather correct especially in regard to its simplicity. If it has a lower efficiency than the best systems in the literature, it presents also the advantage of using a unique water hydraulic machine which is appreciable if high power systems are imagined. First because the water is a natural and neutral fluid for environment; then the power capacity cost (or investment) is much lower using a single hydraulic machine, specially compared to gas compressors and turbines. For example, the cost of compressors and turbines for Huntorf station was around 450€/kW (without including inline heat exchangers cost) [26], in our case, for a small power machine the cost was around 195€/kW. Nevertheless the price of the storage volume needs to be evaluated and minimized; for the cited two high capacity CAES combustion assisted stations, underground caverns were used leading to a very low energy capacity cost. The use of vessels presents a challenge regarding the cost of all the small and medium power storage systems; but it is necessary when no natural cavities are available.

The use of a higher efficiency pump/turbine and operating at higher design powers could fill the gap in efficiency to the best CAES systems with advantage of using no gas combustion or high temperature heat storage systems. The typical pump efficiencies are around 80% and could be even higher for turbines. A higher power system, for the same operating pressure, would lead to higher specific speed machines and thus better efficiencies [27]. Thus, a 55% round trip efficiency seems clearly achievable.

4.1.2. Analysis of PCT cycle

A precise power demand situation was simulated here. Instead of controlling the angular speed of the machine at its best efficiency point, it was controlled to deliver a given prescribed power during the charge and discharge period despite the working pressure variation.

The charging mechanical power was set to 10kW and discharge power to 2.6kW. The initial settings were the same as the ones used for the BEP cycle.

The response of the system in terms of power is shown in Figure 20.

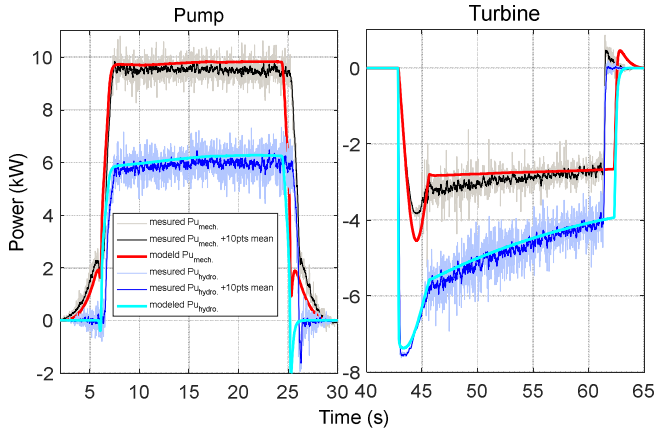

Figure 20: powers during a PCT test

The pump power was maintained almost constant with a maximum gap to the reference power of 5%. During the discharge, the maximum power difference was of 23%. The

turbine operation is much more sensitive to the operating conditions and thus angular velocity. For example in the case of the sensitivity of the torque related to the flow rate variation, for the turbine mode the sensitivity is twice as great as for the pump mode (see chapter 7.5 in [17]). The power control error could be corrected with a closed loop regulation system operating in real time.

The efficiency of the machine is shown in Figure 21. The pump efficiency is maintained relatively high and is almost constant despite the PCT mode whereas the turbine observes a higher variation. The turbine behavior prediction was worse than was for the pump.

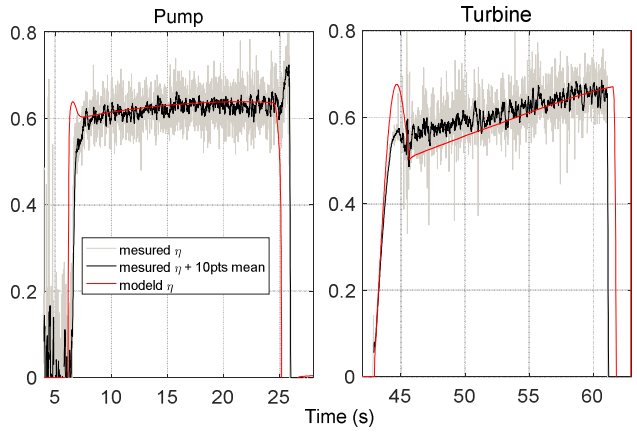

Figure 21: pump/turbine efficiency; PCT mode

The overall efficiency was 28% this case. It has to be underlined that this value is quite close to the one in the BEP case.

5. Conclusion

A prototype of a closed hydro-pneumatic energy storage device using a pump as a turbine has been presented. The pneumatic accumulation efficiency was 84% and the mechanical round-trip efficiency was 31%.. This is a relatively correct efficiency especially in regard to the simplicity of the system and compared to recent HYPES systems in literature. The use of a single reversible machine was demonstrated in a lab scale prototype. This shows the opportunity offered by such machines for ecological, long term and cheap storage solutions.

Two control strategies of the hydraulic machine for a variable operating pressure situation were successfully implemented: best efficiency point and power control strategies. In the first case, the machine efficiency was effectively maintained close to its optimum; in the second case the power was maintained close to the power set-point within a 5% deviation for charging and 23% for discharging. The power control appeared harder to achieve for turbine mode and would probably need to be improved using a closed loop control. Besides the pump mode end control and turbine mode start-up were successfully achieved thus minimizing the valve operation losses and proving the possibility of an off-grid rotodynamic turbine start-up.The dynamic behavior of the system was simulated. Specific parameters of the different modeling sub-domains were empirically calibrated thank to specific tests; the example of the global heat transfer coefficient of the storage vessel was presented. The transient behavior of the system was correctly simulated in various situations and the response time of the storage device was well computed thanks to the presented multi-physic dynamic model. This was made possible by the presented multiphysics dynamic model that considers the strong coupling between hydraulics and mechanics.

The system can be improved in various ways. First, the pneumatic accumulation efficiency and energy density could be increased by achieving quasi-isothermal compression and expansion; that could be achieved by water injections inside the vessel. Then the turbine sensitivity and flexibility can be improved by variable angle external vanes. This could be done in higher power machines. Furthermore, at higher powers, maintaining the maximum pressure, the efficiencies of both modes would be improved; this is related to the increase of the specific speed of the machine. This last point is the main improvement path for such systems.

Regarding the architecture of the system, in order to increase the power flexibility at high efficiency, the use of various staged vessels at various pressures would allow the hydraulic machine operating at the more adequate pressure in function of the appeal power. Also a modular series-parallel piping of various machines with a lower number of stages could help in this same purpose.

At last, an economic analysis should be conducted in order to identify the storage services this kind of systems could answer to. Especially the minimization of the cost of the storage vessels needs to be explored by the right choice of storage pressure and materials. Also the possibility of an open cycle needs to be studied in order to attain competitive energy densities.

6. Acknowledgement

This project was carried out thanks to the financial support of the French agency for environment and energy management (ADEME), which actively induces research on smart grids and storage solutions. Furthermore the technical staff of ENSAM Lille has to be thanked for the important role he played for this project to be realized.

7. Appendices

7.1. Motor PI controller

The required torque of the electric motor was computed by a PI controller; see Figure 22. It takes the reference speed set by the user or the control algorithm. This controller was implemented in the code. In the case of the test bench, this part is integrated to the inverter; the reference speed in that case was given by the Labview program.

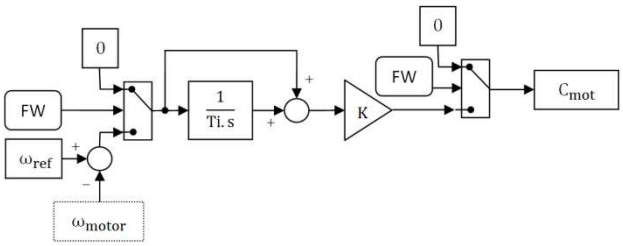

Figure 22: PI controller used to compute the electromagnetic torque

The signal named ''FW'' refers to freewheel mode (1: active, 0: inactive. The threshold of the switch was 0. When freewheel mode is active no torque is applied by the electric motor. The Ti constant was set to 0.2 and K to 40.

7.2. Valve modeling

The pressure applied to the liquid column is computed in a manner that it could achieve the flow rate stopping in almost any situation i.e. closed storage vessel start-up, standard flow closing and those for opening and closing situations. The Figure 23 shows the Simulink program implemented to compute the pressure applied by the valve.

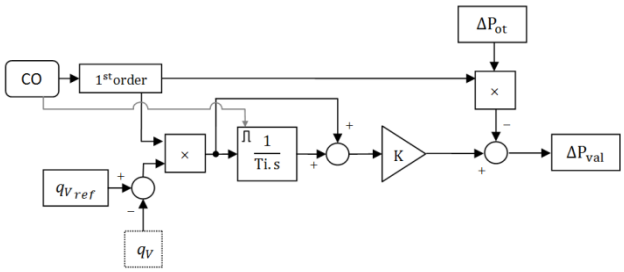

Figure 23: the valve pressure management program

The ''CO'' variable is the closing order (1: close, 0: open). A reset of the integrator of the valve model is needed to enable free circulation after a closing period (grey line). The value of the characteristic time ''Ti'' was 120 and the gain ''K'' had a value of 10.10^6. The value of $q_{V_{ref}}$ was always set to 0. The ''$1^{st}order$'' block represents a first order filter; the integrator of the filter had as initial value the inverse value of its gain. The variable ΔP_{ot} has the value of the $\Delta P_{balance}$ before the subtraction of ΔP_{valve} in equation (4) of the transfer function of Figure 5.

7.3. Power control tables

The look up table values for the PCT mode are given here; pump mode in Figure 24 and turbine mode in Figure 25. For the turbine mode, for a given set of $(Pu_{ref}, \Delta P)$, two angular speed values exist; the one presenting the highest efficiency was used here.

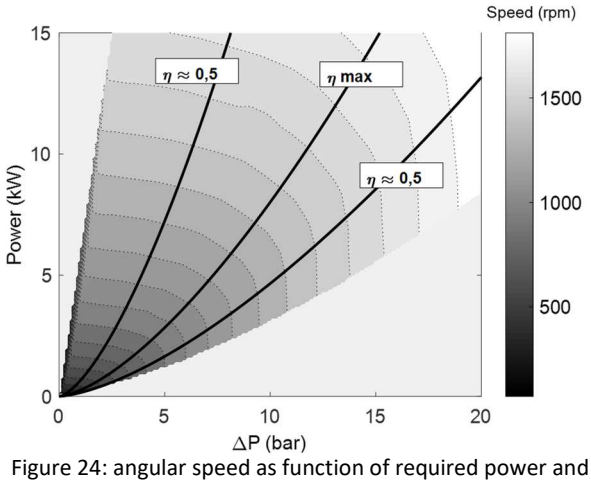

Figure 24: angular speed as function of required power and observed pressure; pump

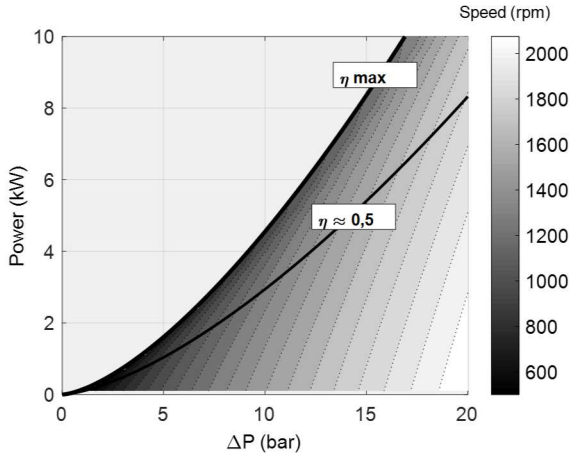

Figure 25: angular speed as function of required power and observed pressure; turbine

8. Bibliography

[1] B. Robyns, B. François and G. M. A. Delille, Energy Storage in electric grids, London: ISTE, 2015.

[2] I. E. Agency, "Tracking Energy Integration," 2019. [Online]. Available: https://www.iea.org/reports/tracking-energy-integration.

[3] J. D. Hunt, E. Byers, Y. Wada, S. Parkinson, D. E. H. J. Gernaat, S. Langan, D. P. v. Vuuren and K. Riahi, "Global resource potential of seasonal pumped hydropower storage for energy and water storage," *Nature Communications,* vol. 11, no. 947, 2020.

[4] M. Budt, D. Wolf, R. Span and J. Yan, "A review on compressed air energy storage: Basic principles, past, milestones and recent developments," *Applied Energy,* no. 170, pp. 250-268, 2016.

[5] M. Finkenrath, *Status and Technical Chalenges of Advanced Compressed Air Energy Storage Technology,* GE Global Research, 2009.

[6] S. Wang, X. Zhang, L. Yang, Y. Zhou and J. Wang, "Experimental study of compressed air energy storage system withthermal energy storage," *Energy,* vol. 103, pp. 182-191, 2016.

[7] S. Zunft, V. Dreißigacker, M. Bieber, A. Banach, C. Klabunde and O. Warweg, "Electricity storage with adiabatic compressed air energy storage: Results of the BMWi-project ADELE-ING," in *International ETG Congress*, Bonn, 2017.

[8] S. Lemofouet-Gatsi, Investigation and optimisation of hybrid electricity storage systems based on compressed air and supercapacitors, PhD, Lausanne: EPFL, 2006.

[9] "Louis Mékarski_1875," [Online]. Available: https://fr.wikipedia.org/wiki/Louis_Mékarski. [Accessed 2020].

[10] "The Project Gutenberg EBook of Scientific American Supplement, No. 799, April 25, 1891," 2004. [Online]. Available: http://www.gutenberg.org/files/11649/11649-h/11649-h.htm. [Accessed 2020].

[11] T. McBride and al., "Systems and method for energy storage and recovery using rapid isothermal gas expansion

and compression". USA Patent US 7,802,426, 28 09 2010.

[12] K.E.Stahlkopf, D.A.Fong, S.E.Crane, E.P.Berlin.JR and AH.P.Abkenar, "Compressed air energy storage system utilizing two-phase flow to facilitate heat axchange". USA Patent US 2011/0115223 A1, 2011.

[13] A. Odukomaiya, A. Abu-Heiba, S. Graham and A. M. Momen, "Experimental and analytical evaluation of a hydro-pneumatic compressed-air Ground-Level Integrated Diverse Energy Storage (GLIDES) system," *applied Energy,* no. 221, pp. 75-85, 2018.

[14] A.G.Olabi, T. Wilberforce, M. Ramadan, M. A. Abdelkareem and A. H. Alam, "Compressed air energy storage systems: Components and operating parameters – A review," *Journal of Energy Storage,* vol. 34, 2021.

[15] C. Nicolet, Hydroacoustics Modelling and Numerical Simulation of Unsteady Operation of Hydroelectric Systems, PhD, Lausanne: EPFL, 2007.

[16] I. Idelcik, Memento des pertes de charge, Eyrolles.

[17] E. Ortego Sampedro, Étude d'un système hydropneumatique de stockage d'énergie utilisant une pompe/turbine rotodynamique, PhD, Lille: ENSAM Lille, 2013.

[18] A. Dazin, G. Caignaert and G. Bois, "Transient Behavior of Turbomachineries: Applicationsto Radial Flow Pump Startups," *ASME, Journal of Fluid Engineering,* 2007.

[19] A. Pourmovahed and D. Otis, "An experimental thermal time constant correlation for hydraulic accumulators," *ASME Journal of Dynamic Systems, Measurement, and Control,* vol. 112, pp. 116-121, 1990.

[20] K.Kadoya, N.Matsunaga and A.Nagashima, "Viscosity and Thermal Conductivity of Dry air in the Gaseous Phase," *J. Phys. Chem. Ref. Dat. Vol.14,* pp. 947-970, 1985.

[21] K.Stephan and A.Laesecke, "The Thermal Conductivity of Fluid Air," *J. Phys. Chem. Vol.14,* pp. 227-234, 1985.

[22] H.K.Kallman, "Thermodynamic properties of real gases for use in high pressure problems. Project Rand," 1950.

[23] D. C. RTeam, *R: A Language and Environment for Statistical Computing,* R Foundation for Statistical Computing, 2011.

[24] F. P. Incropera and D. P. DeWitt, Fundamentals of Heat and Mass Transfer-chap.5.4, John Wiley & Sons, 2002.

[25] M. Cheayb, M. M. Gallego, M. Tazerout and S. Poncet, "Modelling and experimental validation of a small-scale trigenerative compressed air energy storage system," *Applied Energy,* no. 239, pp. 1371-1384, 2019.

[26] C. Kaldemeyer, C. Boysen and I. Tuschy, "Compressed air energy storage in the German energy system-status quo & perspectives," *Energy Procedia,* vol. 99, pp. 298-313, 2016.

[27] B. Jacobsen-GRUNDFOS, "The Centrifugal Pump," 2012. [Online]. [Accessed 2012].